Article:

Wang, J.B., Wang, W.Y., Jewell, G.W. et al. (1 more author) (2005) Design of a miniature permanent-magnet generator and energy storage system. IEEE Transactions on Industrial Electronics, 52 (5). pp. 1383-1390. ISSN 0278-0046

https://doi.org/10.1109/TIE.2005.855658

Design of a Miniature Permanent-Magnet Generator and Energy Storage System

Jiabin Wang, *Senior Member, IEEE*, Weiya Wang, Geraint W. Jewell, and David Howe

***Abstract*—The paper describes a methodology for optimizing the design and performance of a miniature permanent-magnet generator and its associated energy storage system. It combines an analytical field model, a lumped reluctance equivalent magnetic circuit, and an equivalent electrical circuit. Its utility is demonstrated by means of a case study on a 15-mW, 6000-r/min generator, and the analysis techniques are validated by measurements on a prototype system.**

***Index Terms*—Design optimization, energy storage system, miniature permanent-magnet generator.**

NOMENCLATURE

B_r	Radial flux density (T).
$B_{\rm rem}$	Remanence of permanent magnets (T).
e	Emf (V).
f	Electrical frequency (Hz).
g	Airgap length (m).
i	Stator current (A).
J	Stator current density (A/ m^2).
K_h, α	Empirical specific hysteresis loss constants.
K_e	Specific excess iron loss constant.
L	Inductance of stator coil (H).
l_e	Thickness of stator core.(m).
l_w	Axial length of stator coil (m).
$l_{\rm eff}$	Effective axial length of generator (m).
N	Number of turns on stator coil.
p	Number of pole pairs.
p_f	Stator coil packing factor.
P_o	Output power (W).
R	Resistance of stator coil (Ω).
R_m	Outer radius of rotor magnets (m).
R_r	Inner radius of rotor magnets (m).
R_s	Inner radius of stator core (m).
R_w	Outer radius of stator coil (m).
S_l	Equivalent reluctance for inter-pole leakage in stator (H^{-1}).
S_t	Equivalent reluctance of stator tooth body (H^{-1}).
S_a	Equivalent reluctance of assembly gaps in stator (H^{-1}).
S_y	Equivalent reluctance of stator yoke (H^{-1}).
t	Time (s).
T	Electrical period (s).
V_C	DC Output voltage (V).
α_p	Magnet pole-arc to pole-pitch ratio.
α_o	Angular airgap between adjacent stator teeth (°).
ϕ_s	Flux at the stator bore (Wb).
μ_0	Permeability in free space (H/m).
μ_r	Relative recoil permeability of magnets.
μ_{rs}	Relative permeability of stator core.
$\psi_{\rm sc}$	Flux linkage per turn of stator coil (Wb).
ρ	Resistivity of copper (Ωm).
η	Efficiency.
ω_r	Rotor angular velocity (rad s^{-1}).
σ	Electrical conductivity of stator core laminations (S m^{-1}).
δ	Density of stator core (Kg m^{-3}).

Manuscript received February 18, 2003; revised March 5, 2004. Abstract published on the Internet July 15, 2005.

J. Wang, G. W. Jewell, and D. Howe are with the Department of Electronic and Electrical Engineering, The University of Sheffield, Sheffield, S1 3JD, U.K. (e-mail: g.jewell@sheffield.ac.uk).

W. Wang is with Ultralab, Anglia Polytechnic University, Chelmsford, CM1 ILL, U.K.

Digital Object Identifier 10.1109/TIE.2005.855658

I. INTRODUCTION

WITH THE proliferation of portable electronic consumer products and electronic security devices, there is an ever increasing need for relatively low power supplies (typically $\ll$ 1 W). In many applications, on-board power generation would be preferable to the use of batteries, which have a limited capacity and lifetime and contain toxic materials [1], [2]. One means of generating electrical power is to directly convert mechanical energy to electrical energy by incorporating a miniature permanent-magnet generator. The mechanical input power could be derived from intermittent movements, which might be associated with the random motion of a limb, such as the arm, or due to a specific action, such as inserting a key. Linear permanent-magnet generators systems which are capable of extracting and storing energy from both reciprocating and intermittent motion have been reported previously [2], [3]. However, in common with many other direct-drive electromagnetic devices, these tend to have a relatively poor specific power capability since the input speed is limited. Hence, rather than directly converting the kinetic energy to stored electrical energy, it is often advantageous, in terms of both efficiency and specific power capability to initially accumulate the mechanical input energy in a spring. The stored energy can then be discharged at a prespecified rate to drive a high-speed miniature rotating generator [4]. Such an approach is employed in kinetic "self-winding" quartz analog watches, which utilize kinetic energy associated with wrist movements [5], [6]. By way of example, Fig. 1 shows a generator topology which is widely employed in such watches [5]. However, although being conducive to low-cost manufacture, it has a relatively low power density (typically ~ 7.5 kW/m^3) due to a number of factors, including the inefficiency of the magnetic circuit. In order to satisfy potential application requirements for miniature generators, there

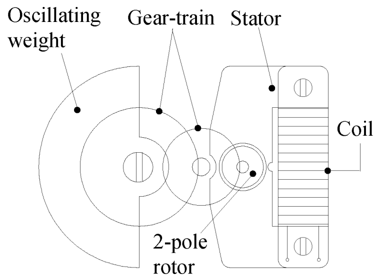

Fig. 1. Schematic of two-pole generator of the type which is currently employed in quartz analog watches.

is a need to improve their design and performance, particularly with regard to power density. This requires the adoption of an alternative topology to that shown in Fig. 1.

When assessing the merits of different generator topologies, it should be borne in mind that, although aspects of machine design are scalable over a wide range of power ratings, there are practical constraints that can compromise various topologies as the machine dimensions are reduced. For example, ultimately, the number of stator coils is limited by the need for terminations and interconnections, which poses practical problems with extremely fine gauge conductors. Furthermore, since an increased proportion of the slot area becomes occupied by insulation, the winding packing factor (i.e., the proportion of the slot which is occupied by copper) can be rather low. An inevitable consequence is that conventional permanent-magnet machine topologies, such a radial-field machines which have a multiphase slotted stator, become inappropriate.

Fig. 2 shows an alternative topology of a single-phase generator which has the potential for a considerably higher power density ($\sim 50\,\mathrm{kW/m^3}$) than the topology shown in Fig. 1, while at the same time retaining much of the simplicity in that it employs a single coil. It comprises a four-pole-pair rotor with parallel magnetized surface-mounted, sintered NdFeB magnet segments and an imbricated-pole stator (also commonly known as a "claw-pole" stator) which is made up of two halves which encircle a single coil. The output power of the generator is rectified by a Schottky-diode bridge, and the electrical energy is stored in a super-capacitor. The paper describes the analysis, design optimization, and testing of such a generator and its associated power conditioning electronics, which are capable of producing 15 mW at 3 V at a nominal rotational speed of 6000 r/min.

II. Magnetic Field Distribution and EMF Prediction

A simple first-order consideration of the performance capability of an imbricated-pole machine suggests that its torque capability increases in direct proportion to the number of stator poles. However, the rate of increase in torque capability with pole number diminishes, due to the increased inter-pole flux leakage in both the rotor magnet/airgap region and between the two sections of the stator core [7]. Indeed, there is an upper limit on the pole number, beyond which the torque capability reduces due to excessive flux leakage.

As a consequence of the relative complexity of the stator geometry, the field distribution is highly three-dimensional (3-D), and although 3-D finite element analysis has been employed for such a machine topology [8], this is inappropriate during the initial stages of design. However, the geometry of the stator is too complex to enable a full analytical field model to be derived. Thus, a method is employed which couples a two-dimensional (2-D) analytical model of a simplified representation of the airgap region to a lumped-parameter equivalent magnetic circuit model of the stator core, in order to derive estimates of the winding flux linkage and impedance and, hence, facilitate initial dimensioning and optimization of the winding, the power conditioning electronics, and the energy storage supercapacitor.

An expression for the airgap field is first derived based on the 2-D model shown in Fig. 3. Although it neglects the axial variation of the field and a number of significant features of the stator geometry, it provides a useful starting point for estimating the magnitude of the flux at the stator bore while accounting for inter-pole flux leakage and flux de-focusing within the magnets, which can be significant when the magnet thickness is comparable with the pole pitch (as is often the case in small machines for which the minimum magnet thickness is usually limited by mechanical considerations). In the simplified model of Fig. 3, the radial component of flux density at any point (r, θ) in the airgap can be shown to be [9]:

$$B_r(r, \theta) = \sum_{n=1,3,5,\ldots}^{\infty} B_n(r) \cos np\theta \tag{1}$$

where $B_n(r)$ is given as shown at the bottom of the page, and

$$M_n = \left(\frac{2B_{rem}\alpha_p}{\mu_0}\right) \frac{\sin\frac{n\pi\alpha_p}{2}}{\frac{n\pi\alpha_p}{2}}.$$

The flux which links the stator, ϕ_s, can be estimated by integrating B_r around a circumferential path located at the stator bore radius $r = R_s$ over an angular displacement α_y, where $\alpha_y = \pi/p - \alpha_0\pi/180$ and α_0 is the angular airgap between adjacent stator teeth. Thus

$$\phi_s = \sum \phi_{np} \cos np\theta \tag{2}$$

$$B_n(r) = \frac{\mu_0 M_n np}{\left[(np)^2 - 1\right]} \left(\frac{R_m}{R_s}\right)^{np+1} \left[\left(\frac{r}{R_s}\right)^{np-1} + \left(\frac{R_s}{r}\right)^{np+1}\right] \times \left\{ \frac{(np-1) + 2\left(\frac{R_r}{R_m}\right)^{np+1} - (np+1)\left(\frac{R_r}{R_m}\right)^{2np}}{(\mu_r+1)\left[1 - \left(\frac{R_r}{R_s}\right)^{2np}\right] - (\mu_r - 1)\left[\left(\frac{R_m}{R_s}\right)^{2np} - \left(\frac{R_r}{R_m}\right)^{2np}\right]} \right\}$$

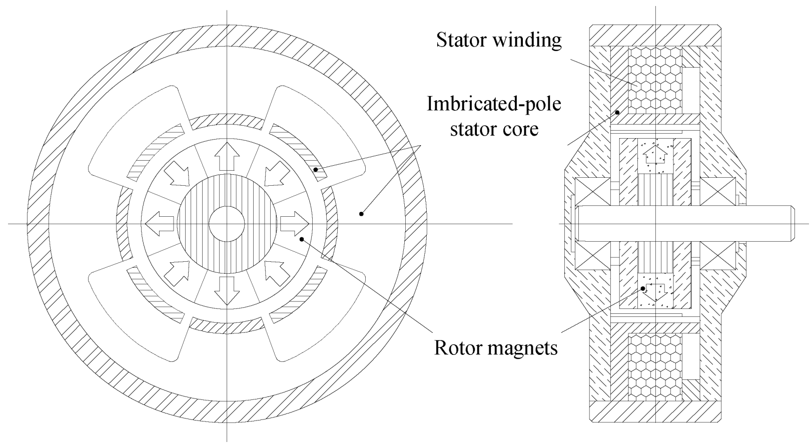

Fig. 2. Schematic of miniature imbricated-pole permanent-magnet generator.

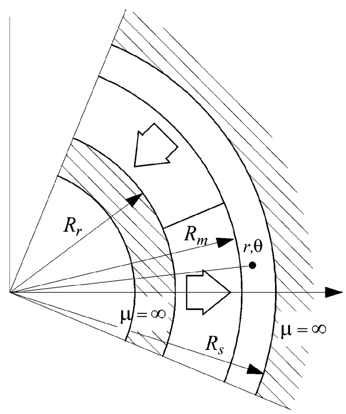

Fig. 3. Analytical field model.

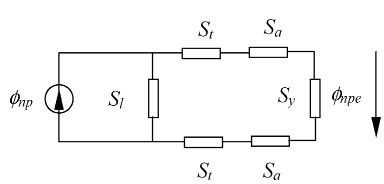

Fig. 4. Lumped-parameter magnetic equivalent circuit.

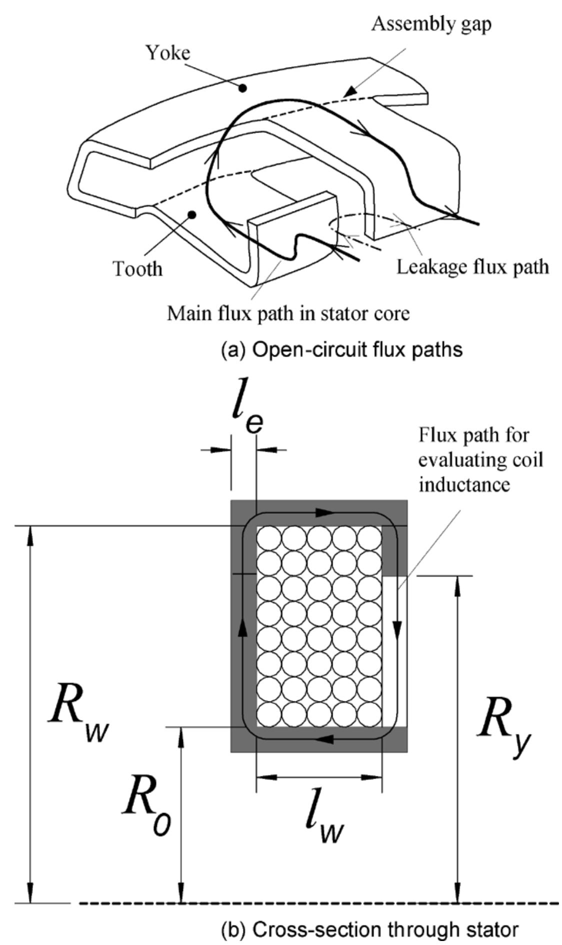

Fig. 5. (a) Open-circuit flux paths. (b) Cross section through stator.

where

$$\phi_{np} = pK_{dn}\alpha_y B_n(R_s)R_s l_{eff}$$
$$K_{dn} = \frac{\sin\left(\frac{np\alpha_y}{2}\right)}{\left(\frac{np\alpha_y}{2}\right)}$$
$$\alpha_y = \frac{\pi}{p} - \frac{\alpha_0\pi}{180}.$$

Having established the magnitude of the flux at the stator bore, the flux which links the stator coil can be estimated using the lumped-parameter magnetic equivalent circuit shown in Fig. 4, which accounts for flux leakage between the stator teeth, saturation within the stator core, and the presence of any assembly gaps between the two halves of the stator (which may have a significant influence given the small dimensions). The magnitude of the flux source in the equivalent circuit is derived from (2). With reference to the flux paths in Fig. 5(a), the reluctances $S_l,\ S_t,\ S_a$, and S_y represent the reluctance of the leakage flux path between adjacent stator teeth, the reluctance of the stator teeth, the reluctance of the assembly gap between the two havles of the stator, and the reluctance of the stator yoke, respectively, and can be calculated as follows:

$$S_l = \frac{0.5R_s\alpha_0\left(\frac{\pi}{180}\right)}{\mu_0(l_w+2l_e)l_e} \tag{3}$$

$$S_t = \frac{(R_w-R_0)}{\mu_0\mu_{rs}w_t l_e} \tag{4}$$

$$S_y = \frac{\frac{\pi R_w}{p}}{\mu_0 \mu_{rs} w_y l_e} \tag{5}$$

$$S_a = \frac{l_{ag}}{\mu_0 w_{ag} l_e} \tag{6}$$

where μ_{rs} is the relative permeability of the stator core, l_{ag} is the length of the assembly gap, and w_t, w_y, and w_{ag} are given by

$$w_t = 0.5(R_y + R_0)\alpha_y$$
$$w_y = 2(R_w - R_y) + l_w + 2l_e$$
$$w_{ag} = \alpha_y R_y.$$

Note that the reluctance due to the stator claws is relatively small compared to the other components and therefore is neglected. Also, the assembly gaps between the stator core pieces are represented in the interface between the teeth and yoke for convenience of the analysis. The influence of saturation in the stator core is accounted for by employing the nonlinear magnetization curve for the ferromagnetic material and calculating the relative permeability μ_{rs} by an iterative approach. Initially, however, the peak flux and the unsaturated value of the relative permeability are used to determine the peak flux density in the stator teeth and yoke. In turn, this allows a revised estimate of μ_{rs} to be determined from the magnetization curve. This process is repeated until the change in μ_{rs} on successive iterations becomes smaller than a specified tolerance. The effective nth harmonic of the flux which links the stator coil ϕ_{npe} can hence be calculated. The total flux which links the stator coil is obtained from

$$\psi_{\mathrm{sc}} = \sum \phi_{\mathrm{npe}} \cos np\theta \tag{7}$$

and the induced emf in each turn of the coil is obtained from

$$e = -\frac{d\psi_{\mathrm{sc}}}{dt} = \sum_n e_n \sin np\theta \tag{8}$$

where

$$e_n = np \cdot \phi_{npe} \cdot \omega_r. \tag{9}$$

III. Design Optimization

In miniature generators of the type shown in Fig. 2, the maximum power capability is generally limited by the impedance of the stator coil rather than by thermal considerations, particularly if the duty cycle is intermittent. Hence, in order to optimize the maximum power capability for a given generator, specifically in terms of establishing the preferred pole number and "split-ratio" (i.e., the ratio of R_m to R_w), it is necessary to determine the impedance of the stator coil. This can be estimated from the simplified stator cross section shown in Fig. 5, for which the coil resistance is deduced as

$$R = K_r N^2; K_r = \rho \frac{\pi (R_w + R_0)}{p_f \cdot l_w (R_w - R_0)}. \tag{10}$$

Assuming that the flux which will result when the stator coil carries current essentially flows around a rectangular path via the yoke and teeth, as shown in Fig. 5(b), the coil self-inductance can be estimated from

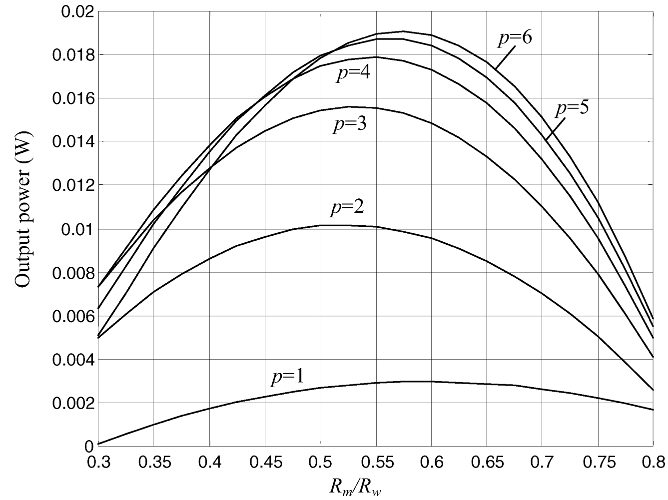

Fig. 6. Generator output power capability as a function of R_m/R_w and number of pole pairs.

$$L = \Lambda_0 N^2; \Lambda_0 = \frac{\pi \mu_0 l_e (R_w + R_0)}{\frac{2(l_w + l_e) + (R_w - R_0)}{\mu_{rs}} + (R_y - R_0)}. \tag{11}$$

The electrical power which is produced by the generator is given by

$$P_o = Nei - Ri^2. \tag{12}$$

Thus, the coil current can be related to the leading dimensions of the generator by

$$i = \frac{(R_w - R_0) l_w \cdot J p_f}{N}. \tag{13}$$

Further, by substituting (8), (10), and (13) into (12), the electrical output power can be calculated for any given combination of pole number and generator dimensions as follows:

$$P_0 = \left(\sum e_n \sin np\theta\right) \cdot J p_f (R_w - R_0) l_w - \rho\pi(R_w^2 - R_0^2) l_w p_f J^2. \tag{14}$$

Fig. 6 shows the calculated variation of the output power capability of a generator running at 6000 r/min as a function of the ratio R_m/R_w and the number of pole pairs, with the remaining design parameters having the values given in Table I. As will be seen, the power capability increases significantly as the number of pole pairs is increased from 1 to 4. However, beyond four pole pairs, the rate of increase in power capability diminishes, since the influence of inter-pole leakage flux becomes more significant. It will also be observed that, for a given pole-pair number, there is an optimal ratio of R_m/R_w which results in maximum output power.

The number of pole pairs also has an influence on the iron loss and, hence, on the efficiency. Thus, the open-circuit iron

TABLE I
SPECIFICATION OF PROTOTYPE GENERATOR

Nominal output voltage (V)	3.0 V
Number of pole-pairs	4
Number of phases	1
Nominal speed	6000 rpm
Output power	15mW

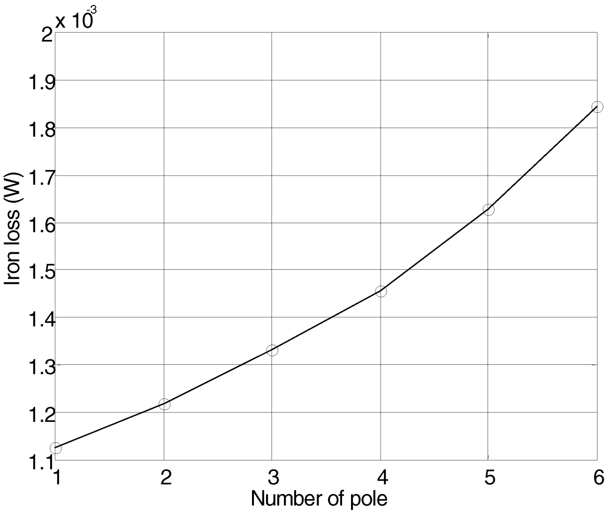

Fig. 7. Variation of open-circuit iron loss as a function of pole-pair number at optimal ratios of R_m/R_w for maximum output power.

loss (i.e., neglecting armature reaction) was estimated using the equation

$$P_{fe} = K_h \cdot f \cdot B_m^{\alpha} + \frac{K_e}{T}\int_T \left|\frac{dB(t)}{dt}\right|^{1.5} dt + \frac{\sigma\, l_e^2}{12\delta}\frac{1}{T}\int_T \left(\frac{dB(t)}{dt}\right)^2 dt \quad (15)$$

to calculate the hysteresis, eddy current, and excess loss components [10]. The total open-circuit iron loss in the stator is obtained by summing the losses in the teeth and stator yoke, in both of which the flux density waveform is estimated by geometrical scaling of the flux density at the stator bore.

Fig. 7 shows the variation of the predicted open-circuit iron loss with pole-pair number when the generator is running at 6000 r/min, assuming that the stator teeth and yoke are 49% cobalt-iron ($\alpha = 2.03$, $K_h = 2.46 \times 10^{-2}$, $K_e = 8.55 \times 10^{-5}$, $\delta = 7.69 \times 10^3\ \mathrm{kg \cdot m^{-3}}$, $\sigma = 2.2 \times 10^6\ \mathrm{S \cdot m^{-1}}$). It is worth noting that the iron loss is relatively small compared to the maximum apparent power capability and that the rate of increase in iron loss with pole number is relatively small (being significantly less than proportional to the increase in fundamental electrical frequency). This is a consequence of an increase in inter-pole leakage flux with increasing pole number (and, hence, a lower overall stator flux) and, more particularly, a decrease in the stator yoke flux density with increasing pole number since

TABLE II
FIXED PARAMETERS EMPLOYED IN THE OPTIMIZATION OF POLE NUMBER AND SPLIT RATIO

Stator current density (J)	4.0 A/mm^2
Stator winding packing factor (p_f)	0.45
Outer radius of stator coil (R_w)	5.0mm
Air-gap length (g)	0.4mm
Axial length (l_w)	1.5mm

TABLE III
DESIGN PARAMETER OF PROTOTYPE GENERATOR

R_r	1.4mm
R_m	2.4mm
R_s	2.8mm
Outer stator radius coil (R_w)	5.0mm
Axial length (including bearings and end-caps)	3.8mm
Number of coil turns	700
Air gap length	0.4mm
Wire diameter	0.050mm

all of the generator designs assume a fixed outer diameter and hence a fixed stator yoke and tooth thickness.

On the basis of Fig. 7 and Table II, a generator with four pole pairs and a R_m/R_w ratio of 0.48 was prototyped, with the other dimensions given in Table III. It should be noted that this ratio of R_m/R_w is slightly smaller than the optimal value of 0.55 in order to accommodate the required number of turns given the available conductor gauge, as will be explained.

Having established the leading dimensions of the generator, it was then necessary to design a coil for maximum power transfer to the load while maintaining a high system efficiency. The output of the generator is connected to a full-wave rectifier which then charges a supercapacitor to store the generated electrical energy, as shown in Fig. 8(a). For the purpose of designing the coil, the generator can be represented as a voltage source in series with the coil resistance and inductance. If the rectifier diodes are modeled as having a fixed on-state voltage drop of V_D in series with a resistor R_D, and the supercapacitor is modeled by a dc voltage V_C in series with an internal resistor R_C, the system may be represented by the equivalent circuit of Fig. 8(b), which consists of an R–L series circuit excited by three independent voltage sources and for which typical current and voltage waveforms are shown in Fig. 9. The output current $i(t)$ of the generator can be calculated from the equivalent circuit as

$$i(t) = \frac{e^{-t/\tau}}{L}\int_{t_0}^{t_0+t} [v(t) - V_C - V_{\mathrm{D}}] \cdot e^{t/\tau} dt, \quad t_0 \le t \le t_0 + t_1$$
$$i(t) = 0, \quad t_0 + t_1 < t \le t_0 + \frac{T}{2} \quad (16)$$

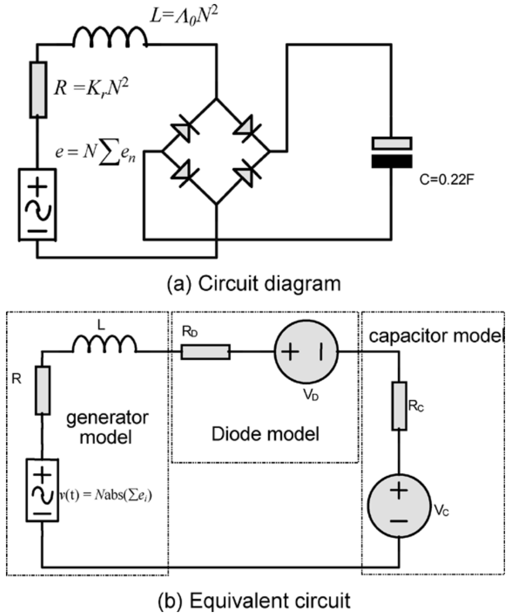

Fig. 8. Rectifier and energy storage circuit. (a) Circuit diagram. (b) Equivalent circuit.

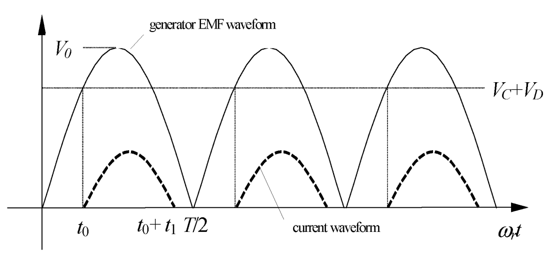

Fig. 9. Typical voltage and current waveforms.

where $v(t)$ is given by

$$v(t) = N \cdot \mathrm{abs}\left(\sum e_n \sin np\omega_r t\right) \tag{17}$$

and $\tau = L/(R + R_\mathrm{D} + R_C)$ is the time constant of the circuit. The conduction period t_1 is determined by solving

$$\int_{t_0}^{t_0+t_1} [v(t) - V_C - V_\mathrm{D}] \cdot e^{t/\tau} dt = 0. \tag{18}$$

The average output power from the generator is, therefore, given by

$$P = \frac{2}{T}\int_0^{T/2} e(t)i(t)dt. \tag{19}$$

Thus, the average input power to the supercapacitor is given by

$$P_S = \frac{2V_C}{T}\int_0^{T/2} i(t)dt. \tag{20}$$

while the power which is dissipated in the equivalent circuit resistances, R, R_D, and R_C is

$$P_{rd} = P - P_S. \tag{21}$$

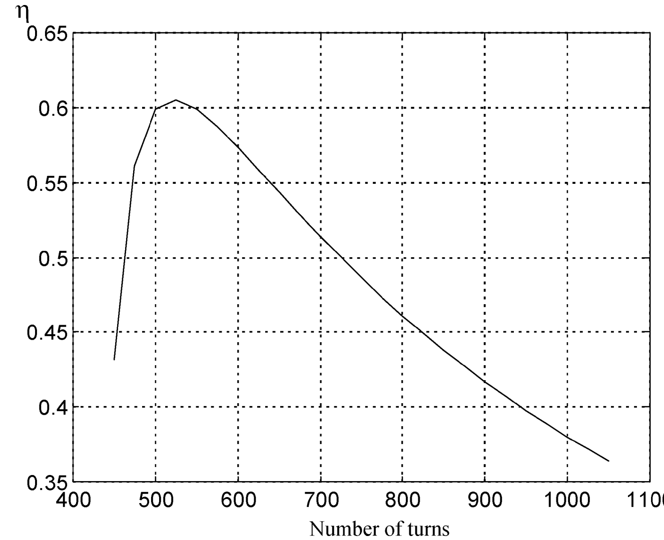

Fig. 10. System efficiency as a function of number of turns on coil, with generator running at 6000 r/min.

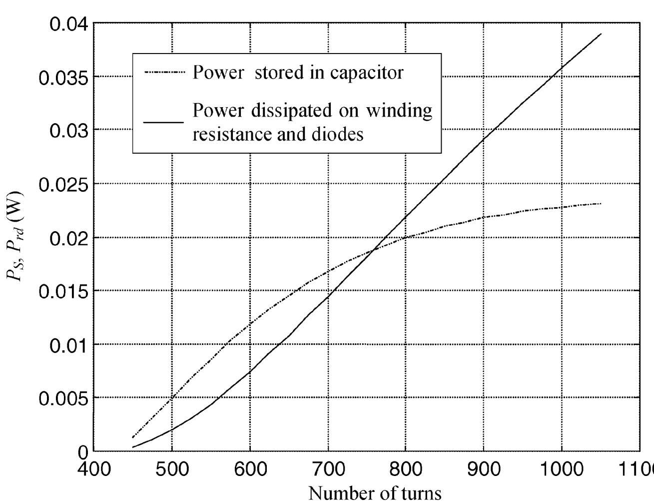

Fig. 11. Power stored in capacitor and dissipated in coil resistance and diodes as functions of number of turns in the stator coil.

The overall efficiency of the system, with due account of the stator iron loss, is given by

$$\eta = \frac{P_S}{(P + P_{fe})}. \tag{22}$$

Figs. 10 and 11 show the variation of η, P_S, and P_{rd} as a function of the number of turns N on the coil for a generator having the parameters given in Table III. As will be seen, the system attains its maximum efficiency when $N = 520$.

However, the average input power to the supercapacitor is then only 6.57 mW. When N is increased to 760, the average input power to the supercapacitor increases to 18.85 mW, although the efficiency also decreases. However, any further increases in N, although increasing the energy which is stored in the supercapacitor, significantly decreases the system efficiency. Therefore, $N = 700$ is deemed to be a suitable compromise between the optimal values for maximum efficiency (520) and maximum power transfer (1040).

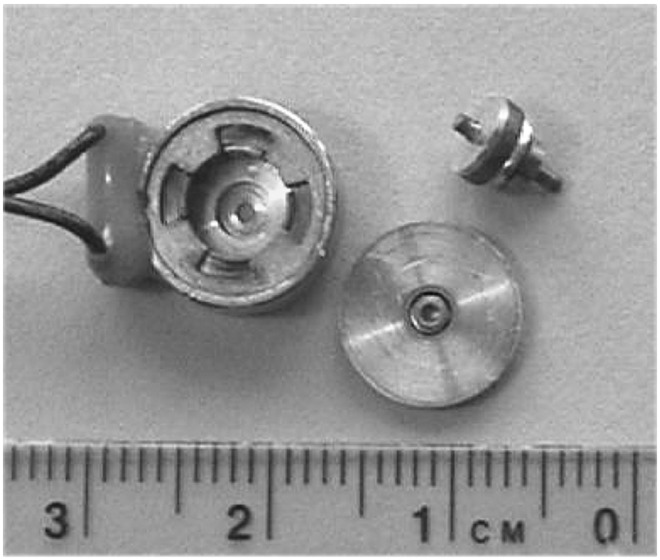

Fig. 12. Prototype generator.

TABLE IV
MEASURED AND PREDICTED COIL RESISTANCE AND INDUCTANCE

	Resistance (Ω)	Inductance (mH)
Measured	155.0	1.48
Predicted	155.8	1.17

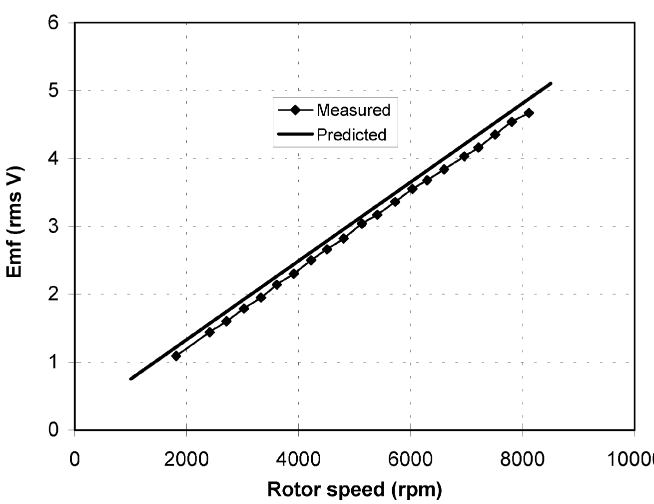

Fig. 13. Variation of measured and predicted emf (rms) as a function of speed.

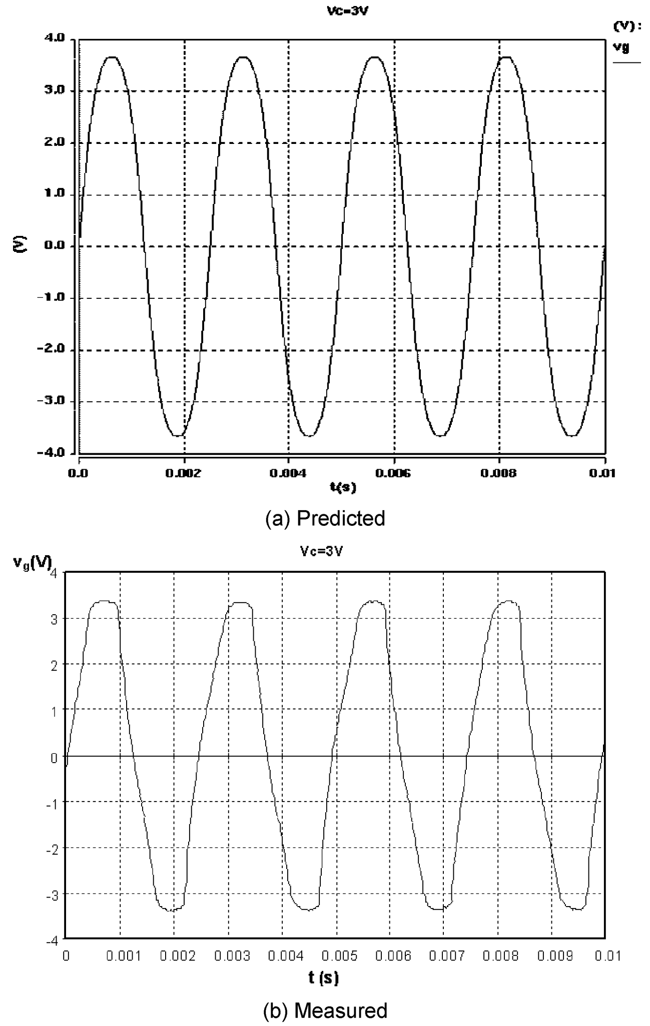

Fig. 14. Predicted and measured generator output voltage with a 0.22-F capacitor. (a) Predicted. (b) Measured.

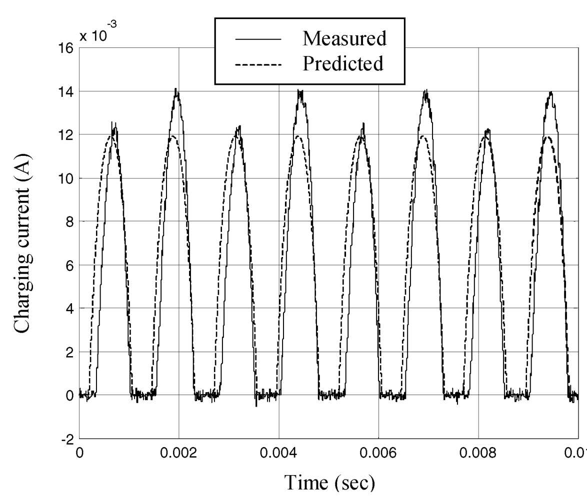

Fig. 15. Measured and predicted charging current waveforms at 6000 r/min and 3 V.

IV. EXPERIMENTAL RESULTS

In order to validate the design and analysis techniques which have been developed, a generator having the design parameters given in Table III was prototyped. Fig. 12 shows the generator, prior to final assembly. The stator is 49% cobalt-iron which was heat-treated to optimize its magnetic properties, while the individual rotor magnets were wire-eroded from sinetered NdFeB (34KC1 from UGIMAG, Inc.).

As will be seen in Table IV, the measured and predicted coil resistance and inductance (measured at the rated fundamental frequency of 400 Hz) are in good agreement. Fig. 13 shows the variation of the predicted and measured open-circuit emf (rms values) with rotor speed, which are also in good agreement. The full-load performance of the generator was measured by connecting a 0.22-F, 3.0-V supercapacitor via a Schottky-diode bridge rectifier, and driving it at 6000 r/min by a dc motor.

Fig. 14 compares the predicted and measured output voltage waveforms. Again, there is good agreement in terms of the amplitudes, although the harmonic content differs slightly. The measured and predicted super-capacitor charging current waveforms are compared in Fig. 15, where the corresponding generator powers are 14.56 and 16.45 mW, respectively. The fluctuation of the measured current waveform results from the asymmetrical magnetic poles due largely to the manufacturing tolerance.

V. Conclusion

A miniature eight-pole permanent-magnet generator with an imbricated multipole stator has been described and analyzed and its performance experimentally validated. A model of the power generation system has been presented, and a design methodology to achieve maximum output power at a specified operating voltage has been developed. It has been shown that the power density is significantly higher than that of two-pole generators of the type which are currently being used in applications such as quartz analog watches. The proposed generator topology may also be employed for multiphase machines and scaled up or down to suit other specific applications, in the mobile communications sector, for example.

References

[1] C. B. Williams and R. B. Yates, "Analysis of a micro-electric generator for microsystems," *Sens. Actuators A, Phys.*, vol. 52, no. 19, pp. 8–11, 1996.

[2] J. Wang, W. Wang, G. W. Jewell, and D. Howe, "Design and experimental characterization of a linear reciprocating generator," *Proc. IEE—Electr. Power Appl.*, vol. 145, no. 6, pp. 509–518, 1998.

[3] ——, "A low power linear permanent magnet generator/energy storage system," *IEEE Trans. Ind. Electron.*, vol. 49, no. 3, pp. 640–648, Jun. 2002.

[4] B. Gilomen, J.-L Béguim, and R. Bugmann, "Mouvement à quartz dont íénergie est fournie par une génératrice, calbre ETA 205.111," *SSC J. dÉtude*, pp. 45–49, 1997.

[5] T. Hara, "Seiko kinetic quartz," in *Proc. 63th Workshop Swiss Soc. Chronometry*, Grenchen, Switzerland, 1995, pp. 71–74.

[6] M. Hayakawa, "A study of the new energy system for quartz watches," in *Proc.. Eur. Conf. Chronometry*, Geneva, Switzerland, 1988, pp. 81–85.

[7] Z. Q. Zhu and D. Howe, "Magnet design considerations for machines equipped with surface-mounted permanent magnets," in *Proc. 13th Int. Workshop Rare-Earth Magnets and Their Applications*, Birmingham, U.K., Sep. 11–14, 1994, pp. 151–160.

[8] I. Ramesohl, G. Henneberger, S. Kuppers, and W. Hadrys, "Three-dimensional calculation of magnetic forces and displacements of a claw-pole generator," *IEEE Trans. Magn.*, vol. 32, no. 3, pp. 1685–1688, May 1996.

[9] Z. Q. Zhu and D. Howe, "Instantaneous magnetic field distribution in brushless permanent magnet dc motors," *IEEE Trans. Magn.*, vol. 29, no. 1, pp. 124–158, Jan. 1993.

[10] K. Attallah, Z. Q. Zhu, and D. Howe, "The prediction of iron losses in brushless permanent magnet dc motors," in *Proc. Int. Conf. Electrical Machines*, 1992, pp. 814–818.

Jiabin Wang (M'96–SM'03) was born in Jiangsu Province, China, in 1958. He received the B.Eng. and M.Eng. degrees from Jiangsu University of Science and Technology, Jiangsu, China, in 1982 and 1986, respectively, and the Ph.D. from the University of East London, London, U.K., in 1996, all in electrical and electronic engineering.

From 1986 to 1991, he was with the Department of Electrical Engineering, Jiangsu University of Science and Technology, where he was appointed a Lecturer in 1987 and an Associate Professor in 1990. He was a Postdoctoral Research Associate with the University of Sheffield, Sheffield, U.K., from 1996 to 1997 and a Senior Lecturer with the University of East London from 1998 to 2001. He is currently a Senior Lecturer with the University of Sheffield. His research interests range from motion control to electromagnetic devices and their associated drives.

Weiya Wang was born in Jiangsu Province, China, in 1957. She received the B.Eng. degree from Jiangsu University of Science and Technology, Jiangsu, China, in 1982 and the M.Sc. degree from the University of East London, London, U.K., in 1996, both in electrical and electronic engineering.

From 1982 to 1993, she was with the Department of Electrical Engineering, Jiangsu University of Science and Technology, where she was appointed a Lecturer in 1988. She was a Research Associate with the University of Sheffield, Sheffield, U.K., from 1997 to 1998 and is currently a Senior Research Fellow with Anglia Polytechnic University, Chelmsford, U.K. Her research interests include electromagnetic devices, miniature mobile robots, meta-level learning, and electronic learning.

Geraint Jewell was born in Neath, U.K., in 1966. He received the B.Eng. and Ph.D. degrees from the University of Sheffield, Sheffield U.K., in 1988 and 1992, respectively.

From 1994 to 2000, he was a Lecturer with the Electrical Machines and Drives Research Group, University of Sheffield, where he now holds an Engineering and Physical Sciences Research Council Advanced Research Fellowship. His research interests cover many aspects of both permanent-magnet and reluctance-based electrical machines and actuators.

David Howe received the B.Tech. and M.Sc. degrees from the University of Bradford, Bradford, U.K., in 1966 and 1967, respectively, and the Ph.D. degree from the University of Southampton, Southampton, U.K., in 1974, all in electrical power engineering.

He has held academic posts at Brunel University, London, U.K., and the University of Southampton, and spent a period in industry with NEI Parsons Ltd., Newcastle-Upon-Tyne, U.K., working on electromagnetic problems related to turbogenerators. He is currently a Professor of electrical engineering at the University of Sheffield, Sheffield, U.K., where he heads the Electrical Machines and Drives Research Group. His research activities span all facets of controlled electrical drive systems, with particular emphasis on permanent-magnet excited machines.

Prof. Howe is a Chartered Engineer, a Fellow of the Institution of Electrical Engineers, and a Fellow of the Royal Academy of Engineering (U.K.).